High-resolution Molecular Dynamics Simulations of the Pyruvate Kinase Muscle Isoform 1 and 2 (PKM1/2)

Quentin DELOBELLE,[†,‡] Théo JAFFRELOT INIZAN,[†] Olivier ADJOUA,[†] Louis LAGARDERE,[†,¶] Frédéric CELERSE,[†,§] Vincent MARECHAL,[‡] and Jean-Philip Piquemal[*,†,‖]

†*Sorbonne Université, LCT, UMR 7616 CNRS, F-75005, Paris, France*

‡*Centre de Recherche Saint-Antoine - Team "Biologie et Thérapeutique du Cancer", Paris, UMRS_938 INSERM, Paris, France*

¶*Sorbonne Université, IP2CT, FR2622 CNRS, F-75005, Paris, France*

§*Sorbonne Université, CNRS, IPCM, Paris, France.*

‖*Department of Biomedical Engineering, The University of Texas at Austin, USA*

E-mail: vincent.marechal@sorbonne-universite.fr,jean-philip.piquemal@sorbonne-universite.fr

Abstract

Glucose metabolism plays a pivotal role in both normal physiological processes and cancer cell growth. The final stage of glycolysis, converting phosphoenolpyruvate (PEP) into pyruvate, is catalyzed by the pyruvate kinase (PK) enzyme. Whereas PKM1 (isoform 1) is mainly expressed in cells with high energy requirements, PKM2 (isoform 2) is preferentially expressed in proliferating cells, including many tumor cells. Structural analysis of both PKM1 and PKM2 is essential to the design of new molecules with anti-tumor activity. To understand the structural dynamics of PKM1 and PKM2, we

performed extensive high-resolution molecular dynamics (MD) simulations using adaptive sampling techniques coupled to the polarizable AMOEBA force field. Performing more than 6 μs of simulation, we consider PKM2 in its various oligomerization states and propose structural insights for PKM1. We particularly focus on the structuring of key sites including the active site and the natural substrate Fructose Bi-Phosphate (FBP) fixation pocket. Additionally, we propose the first high-resolution MD simulation of the biologically active PKM1 and uncover important similarities between the constitutive, tetrameric form of PKM1 and its PKM2 counterpart bounded to FBP. Finally, we analyze the impact of the fixation of TEPP-46, a pharmacological activator, on PKM2 structuring and highlight the structural differences with PKM2 bound to FBP.

Introduction

In normal mammalian cells, ATP is produced by both glycolysis and mitochondrial oxidative phosphorylation (OXPHOS). However, in most tumor cells ATP is produced mainly by glycolysis, even in the presence of oxygen.[1] One of the advantages of preferential activation of glycolysis is the accumulation of metabolic intermediates useful for tumor cell proliferation, such as the biosynthesis of nucleic acids, proteins, lipids, and lactate required to balance the NAD+/NADH redox balance[2] .

Glycolysis is a metabolic process encompassing 10 different steps[3] . It produces two molecules of ATP (adenosine triphosphate), two molecules of pyruvate and two molecules of NADH (Nicotinamide Adenine Dinucleotide) per molecule of glucose. The final stage of glycolysis is a rate-limiting and irreversible phase that converts phosphoenolpyruvate (PEP) to pyruvate. This reaction is catalyzed by pyruvate kinase (PK). There are 4 tissue-specific isoforms in mammals: PKL (Pyruvate Kinase Liver-type) is expressed in the liver, kidney, and intestine tissues, and PKR (Pyruvate Kinase in Red-blood cells) in erythrocytes[4] . Whereas PKM1 (Pyruvate Kinase Muscle isoform 1) is expressed in tissues with high energy requirements

such as brain, heart, and muscle tissues[5] , PKM2 (Pyruvate Kinase Muscle isoform 2) is preferentially expressed in proliferating cells such as embryonic cells and tumor cells[6] . These two isoforms are encoded from the same gene, PKM, which contains 12 exons by alternative splicing generating PKM1 (exon 9) or PKM2 (exon 10).[7,8] PKM1 and PKM2 encompass a total of 531 amino acids while differing by 22 of them[9] .

PKM1 is a constitutive tetrameric active enzyme with a high affinity for its substrate (PEP). Conversely, PKM2 exists in two different forms depending on the cellular compartments: a nuclear dimer associated with a low enzymatic activity and a cytoplasmic active tetrameric form. Allosteric activation of PKM2 is known to occur when it is associated to fructose-1,6-bisphoshate (FBP), which stabilizes the tetrameric form of PKM2.[10] Additionally, the tetramer dissociation favors the accumulation of the PKM2 dimer, which displays pro-tumor activity.[11] The PKM2 tetramer itself is also known to oscillate between two structural organizations: a less active tight (T) form and a fully activated relaxed (R) form. The relative prevalence of these forms is directly associated to the PK immediate environment and the presence of regulating metabolites. PKM1 and PKM2 structural differences tend to explain why PKM1 is not regulated by any kind of allosteric activator.[12] On the opposite, PKM2 enzymatic activity is highly regulated by many endogenous metabolites. It is important to point out that such metabolites can either have the role of an activator (for example: Serine[13] , SAICAR (Succinylaminoimidazole-carboxamide riboside[14] and FBP[15]) or the role of an inhibitor (for example Tryptophane, the T3 thyroid hormone and others[16]). Each monomer of PKM2 contains 3 domains (A/B/C), a short N-terminal region, and an active site. The A domain constitutes the main part of the protein (from residues 44-116 to 219-389). This region is important since the dimeric form of PKM2 is formed through the weak bonding of two of its monomers interacting with this precise region. The B domain is characterized by an external region formed by residues 117-218. It constitutes a part of the active site of PKM2 (PEP fixation) which is structured by an interface between A and B domains. Finally, 44 of the 56 amino acids encoded by PKM2-specific exon 10 are located in

the C domain, which encompasses the allosteric binding site and stabilizes the quaternary structure of the tetrameric form of PKM2. The N-terminal region is localized on residues 1-43 of PKM2[17] .

PKM2's central role in tumor processes makes it a prime target for the design of new anti-tumor molecules and several drugs have been proposed to modulate PKM2 activity and oligomeric state. They either act as an activator promoting the more active R-form (TEPP-46, DASA-58[18]) or as an inhibitor (Shikonin[19] for example). Consequently, it is essential to have a better understanding of the structural dynamics of PKM1 and PKM2 and to identify the conserved sites that could lead to the design of new anti-tumor molecules. Notably, it is especially relevant to investigate the structure of the PKM1 isoform to understand its main structural differences from PKM2 to propose molecules capable of promoting the conversion of PKM2 from the pro-tumor dimer into an active tetramer.

In this paper, we provide all-atom high-resolution molecular dynamics simulations of both PKM1 and PKM2 enzymes and propose a comparative analysis of their key residues and functional sites. In particular, our study focuses on the characterization of the FBP-binding pocket and on the PEP active site which are both closely related to the specificity of activity of both proteins. To provide simulations approaching realistic biological timescales, we use adaptive sampling molecular dynamics coupled to a high-resolution polarizable force field. Thanks to such methodology[20–23] coupled with the use of the GPU-accelerated Tinker-HP molecular dynamics package[24,25] (GPU=Graphics Processing Unit), it is possible to analyze more broadly the structural dynamics and weak interaction profiles[26–28] within these proteins. We therefore evaluate the structural dynamics of PKM1 and PKM2 in their different oligomeric state, notably in the presence or absence of their known effectors.

Materials and Methods

PDB Entries

The PKM1 system was constructed based on its apo tetrameric conformation obtained from the PDB entry 3SRF. We only considered this specific structure since it represents the only known active form of this enzyme. In contrast, PKM2 exhibits a broader range of oligomeric states. Consequently, we considered three initial systems for PKM2: the monomeric (PDB: 1ZJH), dimeric (PDB: 6B6U[29]), and tetrameric (PDB: 3SRH) conformations, all in their apo states. To further investigate the impact of non–covalent interactions of the tetrameric PKM2 with various ligands, we also considered two holo forms of PKM2, associated with 1,6–di–O–phosphono–beta–D–fructofuranose (referred to as FBP, PDB: 3SRD) and TEPP-46 (PDB: 3U2Z[30]), respectively.

Preparation of the Systems

We selected six distinct systems, five corresponding to PKM2 and one to PKM1. For each of them, we removed all non–amino acid elements, retaining only ions, crystal waters, and for the two holo forms, their respective ligands. Subsequently, we prepared these six systems for molecular dynamics (MD) simulations using the polarizable force field AMOEBABIO18.[31,32] While parameters for amino acids as well as water and ions were readily available, standard parameters for accurately describing the dynamics of FBP and TEPP–46 ligands were not present in the literature. Thus, we generated them following the pipeline developed by Ren et al.[33] and employed the Poltype software[34] . We ensured that the generated parameters provided stable MD simulations of each ligand by conducting short MD simulations in a water box. Once we assigned AMOEBA parameters to each molecule, we solvated each system in various cubic water boxes (100 Å x 100 Å x 100 Å for the monomer, 130 Å x 130 Å x 130 Å for the dimer, and 160 Å x 160 Å x 160 Å for the tetramers). Subsequently, we added K^+ and Cl^- ions until reaching physiological pH, known to be optimal for PKM2

in the context of cancer cells[35] .

Conventional Molecular Dynamics

All MD simulations were performed using the Tinker-HP GPU software.[25,36] Initially, each system underwent energy minimization using the L-BFGS algorithm with a Root Mean Square (RMS) threshold of 1 kcal/mol. Subsequently, the systems were gradually heated until equilibration was achieved. This was followed by 5 ns of NVT (canonical ensemble) simulations at 300K, employing the BAOAB-RESPA1 integrator[37] with a timestep of 10 fs, and coupled with Hydrogen-Mass Repartitioning (HMR).[38] The Ewald cutoff parameter was set to 7 Å for Particle Mesh Ewald,[39] and the van der Waals cutoff was set to a value of 9Å . A convergence criterion of 10^{-5} was used for the self–consistent computations of the multipoles. These parameters remained consistent across all subsequent simulations. To further equilibrate the density, we conducted 5 ns of NPT (isothermal-isobaric ensemble) simulations, employing the same thermostat and temperature settings as before. Additionally, we used the Monte-Carlo barostat[40] to regulate the pressure at 1 Atmoshpere. The last frame of each dynamic was taken as the starting point of the production stage, presented in the next section.

Adaptive Sampling Simulations

The primary goal of this study was to capture the largest number of accessible conformations for each active conformation of PKM systems. To achieve this, we employed an enhanced sampling technique known as Adaptive Sampling (AS),[41] which maximizes the exploration of rarely visited regions on the free energy surface associated to representative collective variables obtained through an unsupervised procedure. A notable advantage of this method lies in its unsupervised aspects, making it particularly versatile for studying diverse systems without a strong prior knowledge. AS studies were conducted for each of our six systems using the following pipeline.

An initial pool of structures was generated by running a 20 ns NPT simulation. Dimensionality reduction was then performed on all generated structures by computing the Principal Component Analysis (PCA) components using the sklearn library from Python.[42] Subsequently, the structures were projected into a four-dimensional space using the first four PCA components, as they were found to capture over 90% of the structural diversity.

Following this initial phase, a series of 11 iterations was conducted. In each iteration, 10 structures were selected based on the same density law criterion used by Jaffrelot et al.,[26] who demonstrated robustness in sampling for poorly visited regions. Subsequently, 9 ns of NPT simulations were performed on these 10 selected structures, resulting in a cumulative simulation time of 90 ns per AS iteration. The resulting structures were then added to the pool of conformations, and the process of structure selection was repeated until convergence in the conformational search was achieved.

By conducting 11 iterations, in addition to the initial 20 ns NPT simulation, the study ultimately provided a total simulation time of 1.01 μs per system, amounting to a cumulative simulation time of 6.06 μs for the entire study. The entire post–processing analysis were done using Python script with MDTraj,[43] Numpy[44] , Scikit–Learn,[42] Scipy[45] packages. Further graphical representations with Matplotlib.[46]

Results of the Structural Dynamics Analysis

In this section, we analyzed the large–scale structural dynamics studies of PKM1/2.

Understanding PKM1/2 Structuring during the Oligomerization Process

PKM2

First, we performed comparisons between the Root-Mean Square Deviation (RMSD) and the Radius of Gyration (RG) for PKM1 and the different oligomerization states of PKM2.

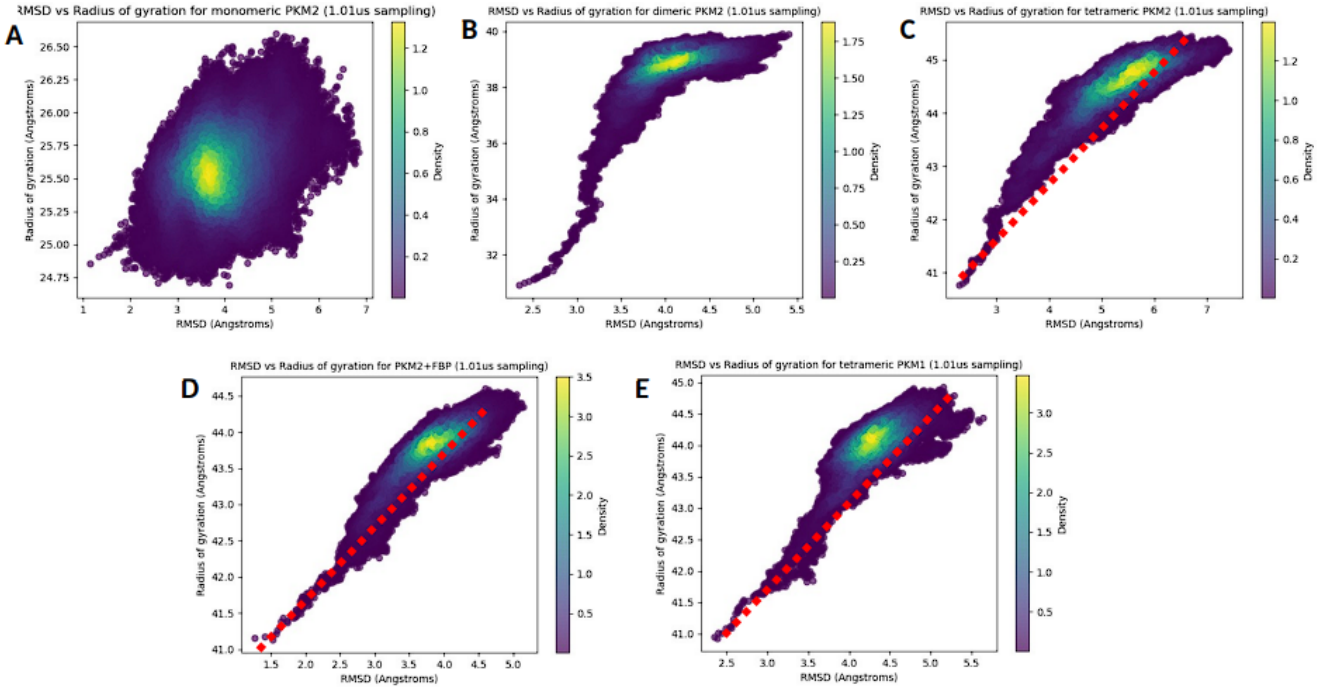

Figure 1: **Global analysis of the RMSD vs RG shows structural changes and of the PKM2 volume during the oligomerization process. We also analyze PKM1/2 profile similarities. (A-D)** Graphical representation of the RMSD/RG analysis for each states of PKM2 molecular dynamics simulation : monomer **(A)**, dimer **(B)** and free-tetramer **(C)** or associated to FBP **(D)**, **(E)** Same representation for the tetrameric form of PKM1.

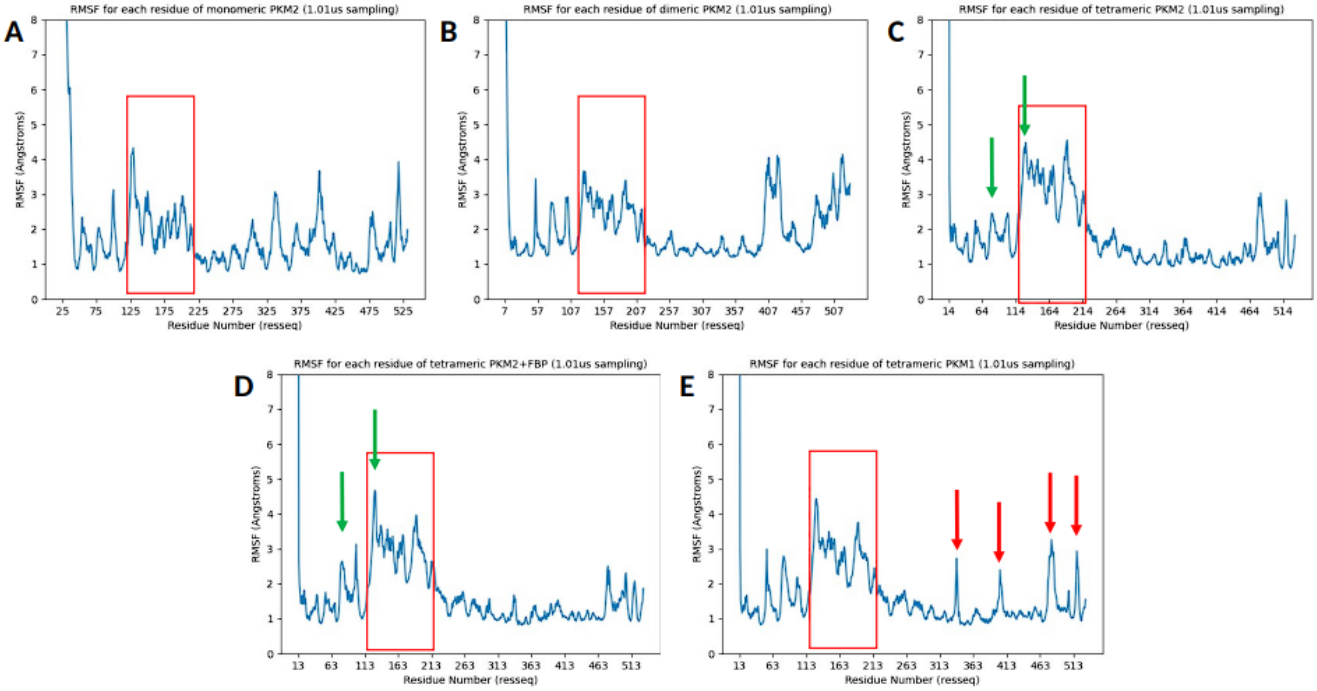

Figure 2: **The RMSF analysis shows PKM2's structuring during the oligomerization and FBP-fixation processes and confirms tetrameric PKM1/2 analogies on key domains. (A-D)** Graphical representation of the RMSF analysis for each state of PKM2 molecular dynamics: monomer **(A)**, dimer **(B)** and free-tetramer **(C)** or associated to FBP **(D)**, **(E)** Same representation for the tetrameric form of PKM1. Here the PKM2 domains contain the following residues : 44-115 for A1, **116-217 for B (red square)**, 218-388 for A2 and 389-531 for C-domain. Local differences between apo and holo PKM2 forms bound to FBP (green arrows), and between holo form of PKM2 bound to FBP and PKM1 respectively (red arrows) are indicated.

The results revealed an increasing correlation of RMSD and RG as PKM2 oligomerization complexified. Figure 1A displays the variations of RG as a function of RMSD in the case of the PKM2 monomer. We observed a specific region of large variations of RMSD and RG (2-7Å and 24.75-26.50Å respectively) during the simulation. High densities of structures were found at RMSD 3.6Å and RG 25.5Å. Overall, the monomeric state was characterized by an important variability as suggested by the absence of global correlation between RMSD and RG. Since the simulations enabled us to explore vast conformational spaces, this indicated that the monomer was poorly structured. This appeared quite different for the dimer (see Figure 1B), for which a narrower distribution of RMSD around 2.5-5.5Å was observed with some larger variations of RG at 31-40Å. Overall a single high density of structures is observed with a significant correlation between RMSD and RG, a sign of the superior structuring of the PKM2 dimer compared to its monomer. In the case of the apo PKM2 tetramer (see Figure 1C), we observed a larger RMSD range compared to the dimer (2.2-7.4Å) which correlated with higher RG values (40.7-45.5Å). Again, a concentration of high densities was found but, this time, an almost linear RMSD/RG correlation was observed. This observation was even more striking when the PKM2 tetramer is bound to FBP (see Figure 1D). Indeed, FBP appeared to have a stabilizing effect on the enzyme structural variability as indicated by the more restricted distribution of RMSD values (from 1.7 to 5.2Å). Again, an extremely dense region of structures (3.5 density at 3.75Å RMSD and 43.75Å RG) was found that demonstrated the full structuring of the enzyme.

PKM1

We compared the different PKM2 structures with the tetrameric PKM1. As shown on Figure 1E, the PKM1 profile appeared to be close to the tetrameric PKM2 when associated to FBP. Indeed, RMSD values were restricted between 2.5 and 5.6Å as RG ranged from 41 to 45Å. Accordingly, an almost identical dense region of structures has been observed compared to PKM2-FBP (3.4 density at 4.25Å RMSD and 44Å RG) as the RMSD/RG correlation was

almost linear.

Altogether, these results confirmed a progressive structuring and correlation between the structural modulation of PKM2 as the oligomerization process increased. Importantly, we observed a close structural proximity between the tetrameric PKM1 and the tetrameric PKM2-FBP.

PKM1/2: Analysis of Residues and Domain Stability during the Molecular Dynamics Simulations

PKM2

The next step of our analysis encompassed the study of the distance between key amino acids of both PKM isoforms as a marker of the flexibility of specific domains. To do so, we studied the Root-Mean Square Fluctuation (RMSF) to quantify the mean deviation for each residue throughout the simulations by comparison with their position in the PDB reference. The first immediate conclusion linked the enzymes' stability to the oligomerization process. Indeed, in the case of the PKM2 monomer (see Figure 2A), our results showed an important flexibility affecting the entirety of the structure. The highest source of flexibility was observed in the B-domain (residues 116-217) which is the most variable going up to RMSF values higher than 4Å. We also observed a large flexibility for three large regions on the A1-domain (residues 45-115) and on additional residues (residues 290-425 and 475-525) that composed a large part of the A2- and C- domains. A structural stabilization was observed for the dimeric state of PKM2 (see Figure 2B). The A2-domain (residues 290-400) losed most of its flexibility with RMSF values centered at 1.5-2Å compared to the monomer values that range beyond 3Å. Still the dimer conserves some structural variabilities on the A1 (residues 50-107) and C-domain (residues 400-457 and 470-531) limiting the full enzyme structuring that seemed

to be only achieved at the level of the apo state PKM2 tetramer (see Figure 2C). Here, the A1- and C-domains residues lost most of their structural variability compared to the dimeric state. A few conserved pockets exhibiting some flexibility were found around residues 30-110 and 470-531 that participate in the structure of the active site and FBP-fixation pocket of PKM2.

It is also important to note that each oligomeric state conserved an important B-domain variability due to its central role in the making of the active site. We then evaluated the allosteric effect of the fixation of FBP on the tetrameric PKM2 (see Figure 2D). If our results showed global RMSF profiles that are extremely close between the holo and apo systems, local differences were observed. Indeed, a further stabilization of the FBP fixation pocket was found at residues 470-531 while relative flexibilities remain for the A1 (residues 70-110) and B-domains and more precisely for certain residues located at 75-80 and 115-120. These residues correspond to key amino acids involved in the active site (see green arrows, Figure 2C).

PKM1

Our results showed a close structural homology between the PKM1 tetramer (see Figure 2E) and the PKM2 holo form bound to FBP, notably in the B-domain. However, some specific regions remain different. Some couples of residues (residues 325-335, 390-405, 470-490, 515-525) present a relatively high flexibility (see red arrows, Figure 2E). Altogether, these results gave a full picture of the local structural effects of the progressive structuring of PKM2 during the oligomerization process. It confirmed the strong structural homologies between PKM2-FBP and PKM1.

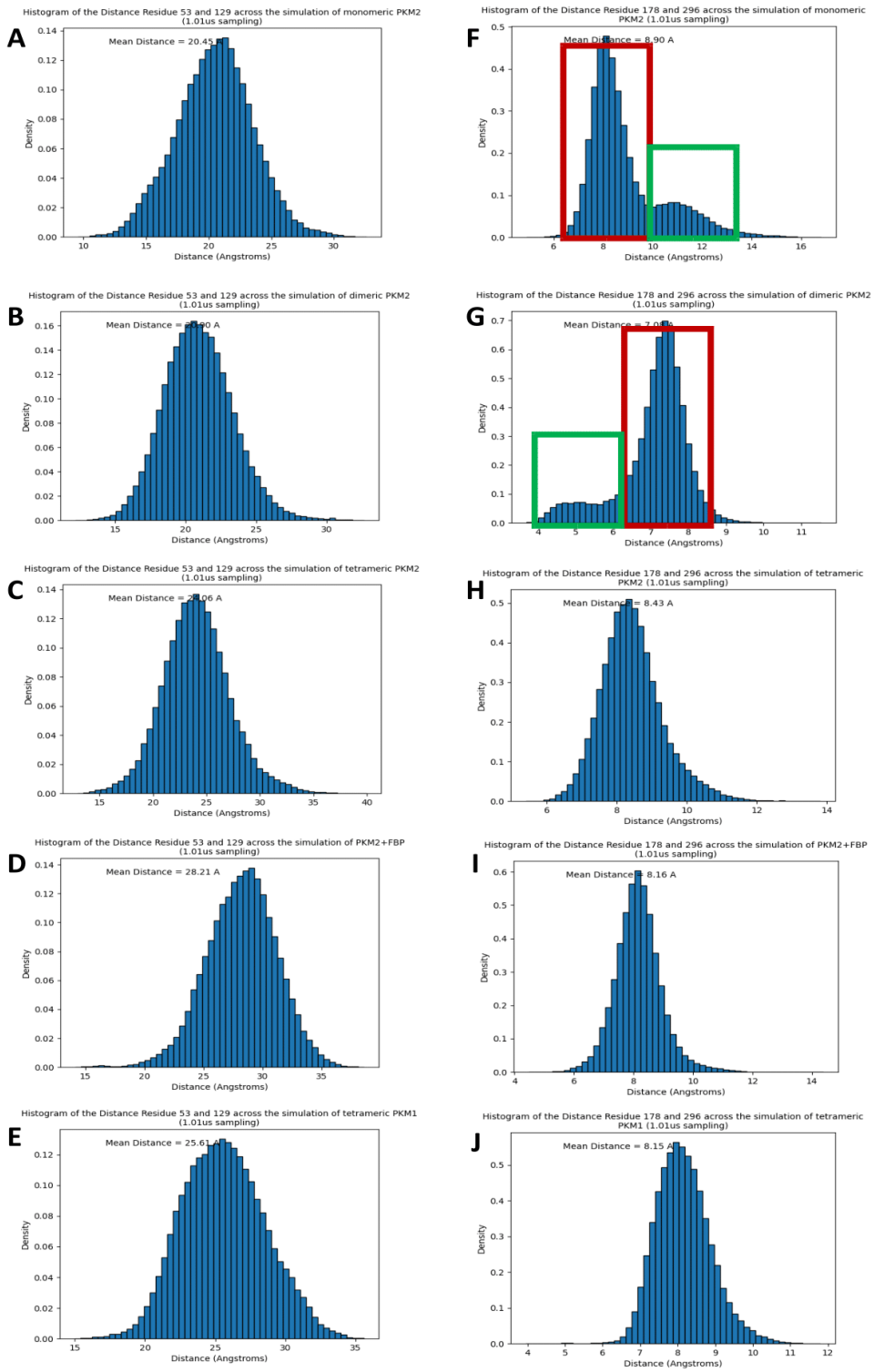

Figure 3: **The structuring of the active site is linked to the oligomeric conformation of PKM1/2. (A-E)** Graphical representation of the distance between residues 53 and 128 (in the active site) for each state of PKM2 within the simulations of the monomer **(A)**, dimer **(B)** and tetramer-apo **(C)** or holo PKM2 with FBP **(D)**, but also for the tetrameric state of PKM1 **(E)**, **(F-I)** Same representation for residues 178 and 296 with the monomer **(F)**, dimer **(G)** and apo **(H)** or holo-FBP **(I)** but also for the tetramer of PKM1 **(J)**

Structuring of the active site and oligomerization state of PKM2

PKM2

We next focused on the PKM2 major key reactivity sites and started by analyzing the active site of the enzyme. To do so, the distances between key couples of residues defining structural markers were studied to evaluate the flexibility of the B-domain. Notably, we measured the distance between residue 53, belonging to the A-domain, and residue 129 belonging to the B-domain. These two residues are located at the external part of the active site. They were chosen to characterize the global motion of the B-domain. To measure the active site structuring, we monitored the distance between residues 178 and 296 (**see Figure 6 in Supplementary Informations**) that are localized at the junction of the A- and B-domains. Simulations showed that the active site was progressively structured during the PKM2 oligomerization process. While the monomeric state (see Figure 3A and 3F) presented a restricted distance between residues 53 and 129 (around 20.5Å), a bimodal distribution of distances was observed between residue 178 and 296 at a distance of 8 and 11 Å. Such bimodal distribution was present in the other PKM2 oligomers. Looking at the dimer (see Figure 3B and 3G), we observed a similar profile to the monomer for the distance between residues 53 and 129. A different bimodal distribution was observed for the distance between residues 178 and 296 (i.e. at the junction of A- and B- domains) with values centered at 5 and 7.5Å, which indicates a more constrained spatial extension of the active site. Then we finally considered the PKM2 tetramer in its apo state (i.e. without its natural ligand, see Figure 3C and 3H). Here, we noticed a higher value of the distance between residues 53 and 129 coupled to a distance between residues 178 and 296 of 8-8.5Å. Such a result indicated a higher flexibility of the B-domain that was linked to a stronger structuring of the active site of PKM2. This appeared fully compatible with the known activities of the different oligomers.[10] When PKM2 was associated with FBP, i.e. forming the holo state (see Figure 3D and 3I), we observed a higher distance between residues 53 and 129 compared to the apo

state (mean value of 28.2Å compared to 24.1Å for the apo-PKM2). The distance between residues 178 and 296 was similar to the apo tetramer but with a slightly narrower distribution centered at 8.25Å. This was in line with the known stability of the PKM2 tetramer when bound to FBP[15] .

PKM1

Finally, we characterized the active site in the tetrameric state of the PKM1 protein to establish a comparison with its PKM2 counterpart (see Figure 3E and 3J). The observed distance profiles were found to be intermediate between the values observed from the apo and holo-FBP state of the PKM2 tetramer. Concerning the external part of the active site, the distance between residues 53 and 129 was lower compared to holo-PKM2 while remaining higher than the distance measured for apo-PKM2, which indicated a higher structuring of the PKM1 active site compared to free-PKM2. In the same line, the junction at the A-B domains (distance between residues 178 and 296) exhibited a very similar profile compared to the holo-PKM2 structure (i.e. mean of 8.15Å vs 8.16Å for the free-tetrameric-PKM2 state). Overall, our data showed a net effect of the FBP allosteric effector on tetramer active site structuring that appeared relatively similar to the PKM1 isoform.

Structural Dynamics of the FBP-fixation pocket : Allosteric and Oligomeric modulations

PKM2

Here, we compared the structuring of the region that contains the FBP-fixation site in PKM2 and the corresponding region in PKM1. The distance between residue 433 and 518 has been studied to evaluate the global flexibility of the FBP-fixation site since these residues are located at the extrema of the pocket (**see Figure 7 in Supplementary Information**).

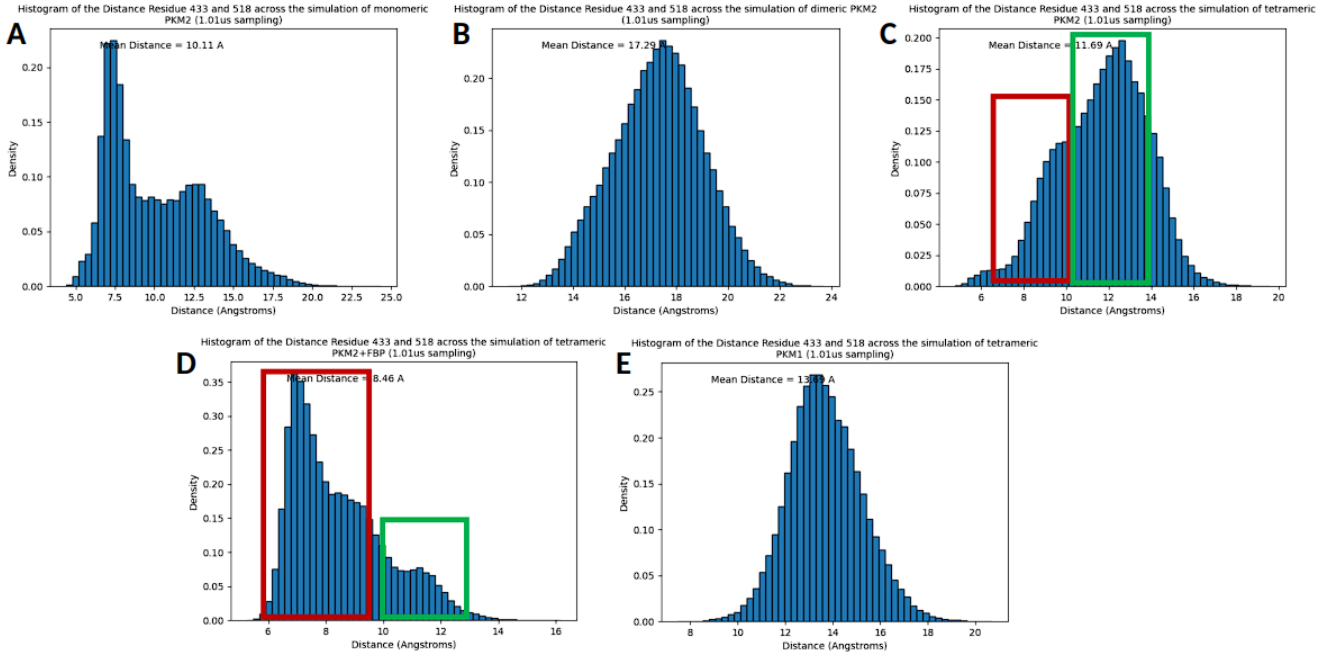

Figure 4: **Global structuring of the FBP-fixation pocket during PKM2 oligomerization and FBP-docking process and comparison with PKM1 possible fixation site.** **(A-D)** Graphical representation of the distance between residues 433 and 518 (localized at the FBP-allosteric pocket) for each oligomeric state or condition of PKM2 molecular dynamics with the monomer **(A)**, dimer **(B)** and tetramer-free **(C)** or associated with the allosteric molecule FBP **(D)**, **(E)** Same representation for the tetrameric form of PKM1.

We first compared each possible PKM2 oligomeric states used for our simulations. The results obtained on the monomer (see Figure 4A) showed a highly variable profile of distances with a large density of structures centered at 7.5Å that were also coupled to a very large proportion of higher distance at 8.5-13Å. This provided a good indication of the likely absence of this pocket within the monomeric state. Considering the PKM2 dimeric form (see Figure 4B), we observed higher distances compared to the monomeric state. More precisely, a unique and wide distribution was found with distances ranging from 13 to 21Å which was not in favor of an overall well-structured FBP-fixation pocket since computed distances were really high. Then, we observed a bimodal distribution for the distance between amino acids 433 and 518 distance in the apo PKM2 (see Figure 4C, red an green boxes), with a more preponderant population of structures centered at 12.5Å (at 0.2 density) and a second one at 9.5Å (at 0.115 density). This particular distribution was a signature for the co-existence of two distinct states for the tetrameric PKM2. For PKM2 bound to FBP, we noticed a complete inversion of the observed 2-states distribution compared to the apo-PKM2 state (see Figure 4D). In this case, a major population of structures was centered around a mean distance at 8.5Å (0.18 density) whereas a second population was center at 7Å (0.36 density). As expected, FBP played a major role on the structuring of the FBP fixation pocket.

PKM1

The characterization of the putative FBP-fixation region for the PKM1 protein was performed to compare it to its PKM2 counterpart. The data obtained from this tetrameric state (see Figure 4E) showed a distribution of the distance between residues 433 and 518, that was centered at 13.7Å, a much higher distance than the one observed in apo-PKM2 (i.e. at 11.7Å) and in holo-FBP PKM2 (i.e.at 8.46Å). These data confirmed that the putative allosteric site in PKM1 did not appear to be structured enough to have a viable fixation pocket to bound FBP.

PKM2 associated with the TEPP-46 pharmacological activator

To conclude our structural analysis, we studied the structure dynamics of PKM2 associated with TEPP-46, a pharmacological effector known to be an activator of PKM2. First, the RMSF data (see Figure 5A) gave a similar profile to the one observed for PKM2-FBP with minor local differences (residues 390-405 and 470-490), that were located in the areas of interaction with TEPP-46 and in some residues for FBP-fixation pocket respectively. As for the studies of PKM2 tetramers, the B-domain (residues 116-217) retained the same distance profile as the one observed in the presence of FBP. To have more structural information, we studied in more detail the active site of PKM2 (see Figure 5B). For the distance between residues 53 and -129, similarities were noted between PKM2 bound to FBP and PKM2 linked to TEPP-46. The data showed that the distance at the A-B junction (residues 178 and 296) was very similar to the one observed when PKM2 was linked to FBP. Conversely, the fixation of TEPP-46 had an opposite effect on the movement of the B-domain. Indeed the distance between amino acids 53 and 129 was reduced and exhibited a bimodal profile at 12 and 19Å indicative of a closed proximity between the B- and the A- domain. Altogether, this was consistent with a better enzymatic activity for PKM2 bound to TEPP-46 than for the PKM2 tetrameric-free state. Finally, the structural analysis of the FBP-pocket (see Figure 5C) showed that the distance between residues 433 and 518 was extremely close (i.e. centered at 7.5Å) compared to the one present in the FBP-PKM2 structure. However, in the case of PKM2 bounded to TEPP-46, no ligand was localized in this space since the TEPP-46 fixation pocket is located in a different region of PKM2.

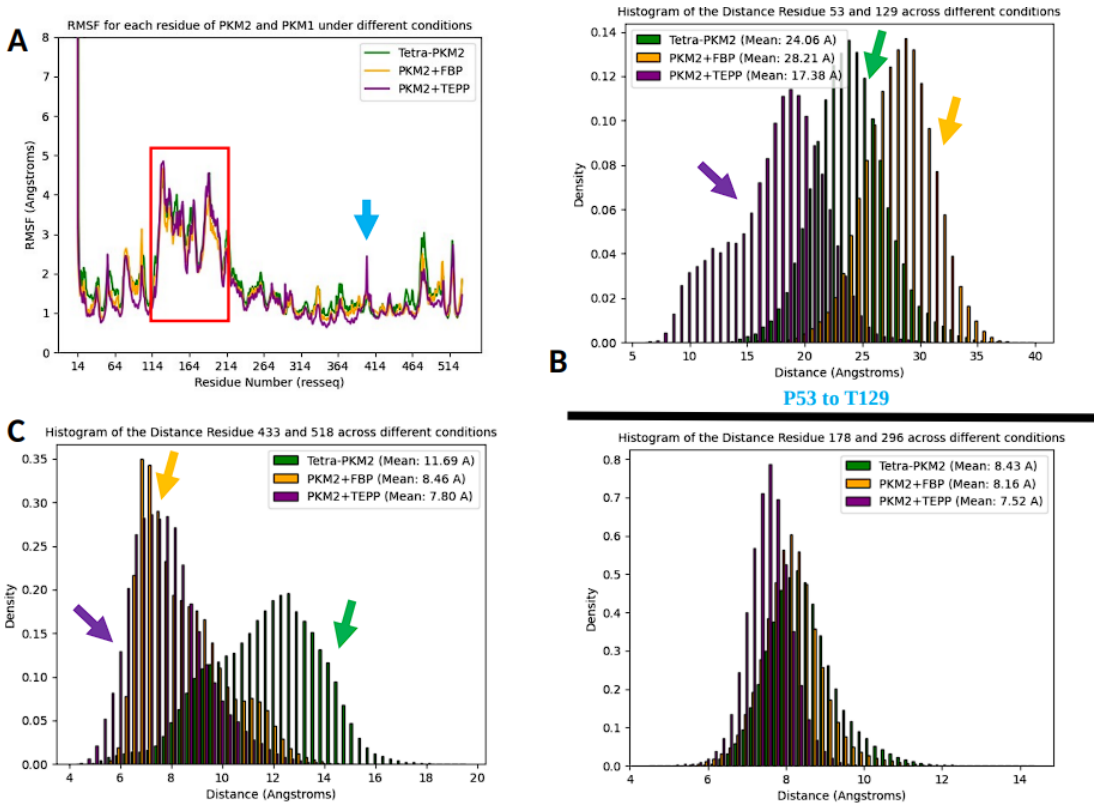

Figure 5: **Structural data associated to the TEPP-46 fixation on a tetrameric PKM2. (A)** Graphical representation of the RMSF analysis, **(B)**, distance between residues 53 and 128 (in the active site) and **(C)** distance between residues 433 and 518 (localized at the FBP-allosteric pocket) for different tetrameric state of PKM2 with or without natural or pharmacological effectors.

Discussion

We first compared the different oligomerization states of PKM2, ranging from monomer to tetramer and unrevealed an increasing stabilization of the protein up to the holo tetramer state for which a gradual linear correlation between RMSD and RG was observed. Such a correlation is therefore a good marker of a conformational transition that allows to maximize the structuring of PKM2. These results are partially validated by comparing it to the experimental work of Ponnusamy[47] that provided RG and RMSD results on a PDB structure of PKM2 that is similar to our simulations monomer data. Overall, our results clearly correlate with the experimentally observed differences in enzymatic activity.[48] The dimeric form is less active whereas the tetrameric form of PKM2 exhibits a higher affinity for its PEP substrate and a better enzymatic activity. This increase of activity between each state is strongly linked with the progressive structuring of the active site. Additional information can be found directly by studying the RMSF evolutions: starting from an extremely variable monomeric state, the dimer stabilized itself while the tetrameric form of PKM2 bound to FBP exhibits the highest level of structuring. Nevertheless, the B-domain (residues 116-217) still shows a high flexibility for each oligomeric state. Such flexibility is lower for the tetramer compared to the dimer and could be an explication for the difference of affinity with its substrate which is found in favor of the tetramer.[49] Further analysis of distances at key residues of the active site (53-129 and 178-296) supports this hypothesis. Indeed, the bimodal and more narrow value at the inside part of the active site of the dimeric form is extremely different from its tetramer counterpart. In the same line, the dynamically unstable internal junction (i.e. at the active site) of the monomer confirms the experimental data from the study of Guo et al[50] who showed reduced enzymatic activity of the monomeric state. To conclude this discussion on the oligomeric forms of PKM2, it is important to look at the amino acids localized at the FBP-fixation pocket. While the monomer and dimer exhibit large structural pocket variations preventing it from any activity, the tetramer exhibits a bimodal distribution of the structures of the FBP-fixation pocket. This is observed

for the free-tetramer where the reference Gly518 residue, which is chosen for the distance measurement, is localized in a well-known regulation-loop which has been experimentally shown to be highly flexible.[51] Such flexibility is related to interactions of close amino acids including Trp515 and Arg516 that are implicated into the regulation of PKM2 being able to generate a less active tetramer (i.e. the T-state) and the more active form (i.e the R-state). For the T-state, this loop is externalized from the FBP-fixation pocket and is able to form hydrogen bonds with the other chain nearby. This is also shown by our data and associated to higher 433-518 distances. On the opposite, for the R-state, the hydrogen bonds are lost since the loop that includes Gly518 is getting closer to the FBP fixation pocket exhibiting closer distances within the simulation in agreement with previous experimental data[51] . The two states observed for the tetramer in the simulations are consistent with the experimentally observed equilibrium between the two states of the tetramer PKM2, namely the R and T states[51] . Taking into account every aspect of this comparison, our study provides a good insight for the progressive structuring of PKM2 during the oligomerization process. In line with biological data[52] , our results confirm its link with the overall enzyme activity as the PKM2 oligomerization should have a regulating role in the control of the cellular metabolism but also in the context of cancer. Indeed, the prevalence of the PKM2 dimeric state in cancer correlates with its reduced enzymatic activity compared to the tetramer.[53]

The second insight brought by our study is materialized by the role of the natural FBP ligand in the structural regulation of PKM2 key pockets. First, the RMSD/RG profiles between the PKM2 apo and holo states exhibit a strong linear correlation in the holo-PKM2 condition. This is linked to the strong structuring effect of FBP on the tetramer which is confirmed by RMSF data. If they show very similar global profiles between both states, the holo state of PKM2 is nevertheless further stabilized in the C-terminal part of the protein that contains key residues for the fixation of FBP. It is important to note that even if FBP is docked into the PKM2 tetramer, the B-domain conserves its flexibility, especially in some

small regions (Asn75, His78, Asp113, Thr114 and Arg120) implicated into the structuring of the active site. Such differences could explain the better substrate accessibility for the active site through the allosteric effect of FBP. This is consistent with some previous theoretical results obtained on shorter molecular dynamics simulations on only one chain of two tetrameric crystal structures.[54] The distance analysis of residues 53-129/178-296 localized at the active site validates this assumption. Overall, our results confirm that the fixation of FBP is important to maximize the structuring of PKM2 active site thus allowing better enzymatic activity. Concerning the analysis of the FBP-fixation pocket itself, our results show the bimodal state of the tetramer PKM2 which reflects the existence of two different states, the T- and R- states. In the case of the holo-FBP form of PKM2, the residues that are constitutive of this pocket are less distant than in the apo state, an indication of structuring. Our results confirm some previous biological works of Morgan et al.[10] concerning the effect of FBP on the R/T equilibrium of tetrameric PKM2 in human and in parasites.[55] This is further validated thanks to our modeling of a tetrameric state bound to the TEPP-46 pharmacological activator that is reminiscent to the one obtained with FBP. This is in line with biological data.[18] Nevertheless, it is important to point out that the fixation region of TEPP-46 is localized in a different pocket than FBP inside PKM2 structure and this could be a reason why the B-domain is more rigid in this case. However, TEPP-46 binding is still able to induce a good structuring of the active site thanks to a stable binding after adding it to the structure. Interestingly, having a profile of the FBP-fixation pocket close to the PKM2+FBP condition even in the absence of FBP could explain the "FBP-like effect" of TEPP46 observed in the biological data[18] .

Lastly, we also performed a characterization of the tetrameric state of PKM1 which is poorly described in the structural literature compared to PKM2. Our RMSD/RG analysis reveals the proximity of PKM1 with those of its PKM2 tetrameric counterpart, with or without FBP. PKM1 exhibits an intermediate profile between the holo and apo PKM2 forms. This

is consistent with the fact that PKM1 is known to be a constitutively tetrameric protein that possess an enzymatic activity similar to FBP-PKM2.[56] Our RMSF data reveal the relative similarity of PKM1 with holo-PKM2 regarding the B-domain and to small key amino acids related to the active site. Nevertheless, some regions have a higher RMSF flexibility compared to holo-PKM2. The first small region more flexible in PKM1 compared to PKM2 is located at key residues 325-335 and contain the amino acid Thr328 that is implicated in the structuration of the PKM1/2 active site. Concerning regions at residues 470-490 and 515-525, both of them contain key amino acids implicated in the structuring of the PKM2 FBP-fixation pocket of PKM2 where their flexibility is reduced. One hypothesis could be that these unstable regions present in our PKM1 simulations could block the formation of an effective FBP-pocket. Presently, no structural or experimental data support the effect of FBP on PKM1 except for some fixed data of the regulatory loop on an initial crystal structure comparing FBP-fixation pocket of PKM1 and PKM2 from Dombrauckas et al.[17] . The last small region located at residues 390-405 is specific of PKM1 since it is encoded by the two different exons in PKM1 and PKM2. This result is surprising but coherent since this region contains less flexible residues on the PKM2 counterpart specific exon (i.e. Tyr390, Gln393 and Leu394) that participate in the binding of known activators of PKM2 such as TEPP-46 and DASA-58.[30] One hypothesis could be that this relative instability of this key region is one of the reason that makes this specific pocket a target for PKM2 and not for PKM1. To investigate the PKM1 active site, we have chosen to study the distance between amino acids that are present on both PKM isoforms. Our study is in agreement with the biological data indicating that PKM1 is an active enzyme (structured active site) and where its B-domain conserves a relative flexibility. It is in coherence with the results obtained for PKM2 since no exon-specific residues are implicated in the structuring of the active site of both proteins.[17] Finally, there is the question of the existence (or absence) of the FBP-fixation pocket for PKM1 since no experimental data have shown any direct allosteric effects of FBP on PKM1. Our results add further validation to this hypothesis since distances for

PKM1 tetrameric state are much higher that the PKM2 state bound to FBP. Indeed PKM2 (apo and holo-FBP) have two possible state, this is not the case for PKM1. The distribution of distances shows an absence of stable structuring of a putative FBP-fixation pocket in this region of PKM1. This data allows then to correlate the absence of allosteric effect on PKM1 with the absence of "allosteric pocket" in link with exon-specific residues that are absent on the PKM1 isoform[6] .

Conclusion

High-resolution μs-scale molecular dynamics simulations were performed on both PKM1 and PKM2 enzymes using atomistic models. Whereas PKM1 is only expressed as an active tetramer, PKM2 models range from a monomer to a tetramer isoform. Such models allowed for an extensive study of the regulation of key domains such as the active site and the FBP allosteric pocket. First at a global level, the PKM2 oligomerization process, which ranges from the monomer to the tetramer, shows a progressive structuring while maintaining some flexibility on its B-domain which is intimately linked to the active site structuring. Our results clearly highlight the superior structuring of the PKM2 tetramer state compared to its monomer and dimer counterparts. In addition, the PKM1 global structural profile presents a strong homology with the PKM2 tetramer bounded to FBP, despite the observation of small regions exhibiting higher flexibility. This is confirmed by strong structural similarities in the active site region. Moving then to the FBP-fixation pocket, and as could one expect, the latter appears to be strongly affected by the structuring presence of the FBP ligand. Indeed, the binding of FBP tends to select the most active R-state which exhibits the most structured active site among the two states equilibrium of this pocket when FBP is not present inside the tetramer. In parallel, the putative PKM1 FBP-fixation pocket tends to

possess a larger volume compared to the FBP-pocket of PKM2 thus indicating an absence of FBP fixation while still conserving a structured active site in agreement with biological data.

These new findings on the specificity and structure of each known oligomeric form of PKM1/2 isoforms add further knowledge in the perspective of finding new molecules to modulate the enzymatic activity of the PKM enzyme. Indeed such findings would be innovative in cancer therapy but also in the case of viral infection since PKM2 has been shown to participate positively in viral replication in Human-Immunodeficiency Virus (HIV)[57] or the pro-tumoral Epstein-Barr virus (EBV)[58] . Thus, future research focusing on the structural dynamics of PKM isoforms will need to concentrate on finding possible cryptic pockets, on locating key amino acids implicated in the FBP allostery and on already known effector-fixation pockets like the one involved in TEPP-46 that could have a potential impact on drug discovery since the equilibrium between dimeric and tetrameric state of PKM2 is primordial for its pro-tumoral and pro-viral effects. It would be also interesting to perform additional simulations involving PKM1 with FBP to further validate the absence of allosteric effect while further characterizing key residues implicated into bonds for the transition between dimer and tetramer of PKM2. Furthermore, while this study is centered on the structural aspects of these proteins, further validation with experimental data would be needed to validate some of theoretical findings. This involves some experiments using mutagenesis targeting key residues (FBP-pocket, tetramerization region...) but also the testing of drugs. Such studies would be another major step to design molecules specific of PKM2 and aimed at conducting new anticancer and antiviral therapy.

Acknowledgements

This work was made possible thanks to funding from both MESRI financing of the Programme Doctorale Interdisciplinaire en Cancérologie (PDIC) and the European Research

Council (ERC) under the European Union's Horizon 2020 research and innovation program (grant agreement No 810367), project EMC2. Computations have been performed at GENCI (IDRIS, Orsay, France and TGCC, Bruyères le Chatel) on grant no A0130712052.

Competing interest

The authors declare no competing interests.

Additional information

Additional informations can be find in SI.

Supplementary Figure

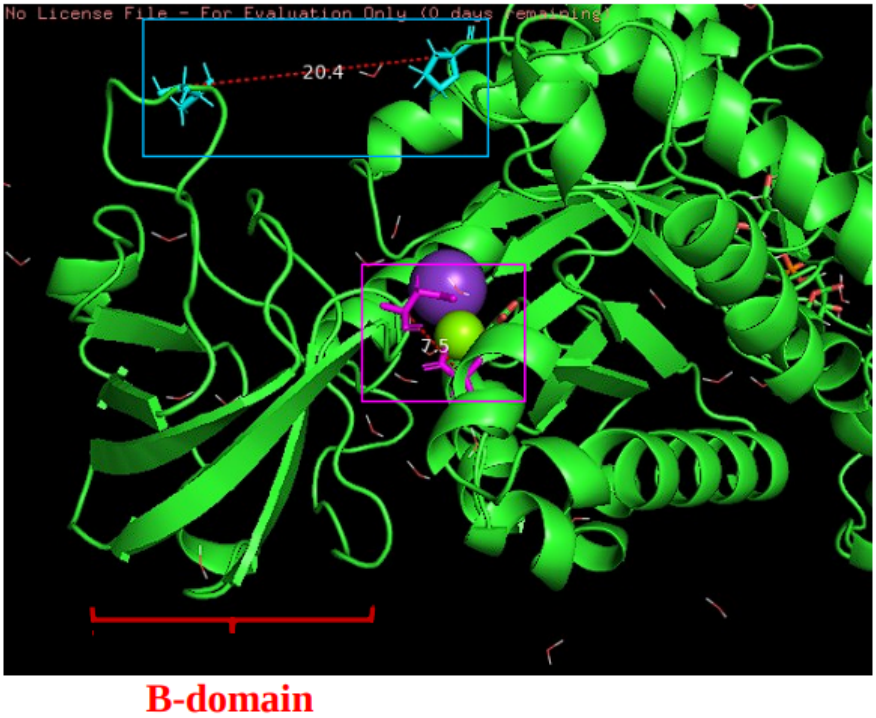

Figure 6: **Structural representation of the active site of PKM2.** Cartoon model representing a single monomer of the PKM2 tetramer associated with FBP. Here, the two couple of residues **P53 to T129 (between regions A and B) and D178 to D296 (close to the A-B junction at the base of region B)) are highlighted respectively in blue and pink** to characterize their importance in the overall structural dynamics occurring at the active site of the protein, which is localized between the A1 (right side) and B-domains (left-side)

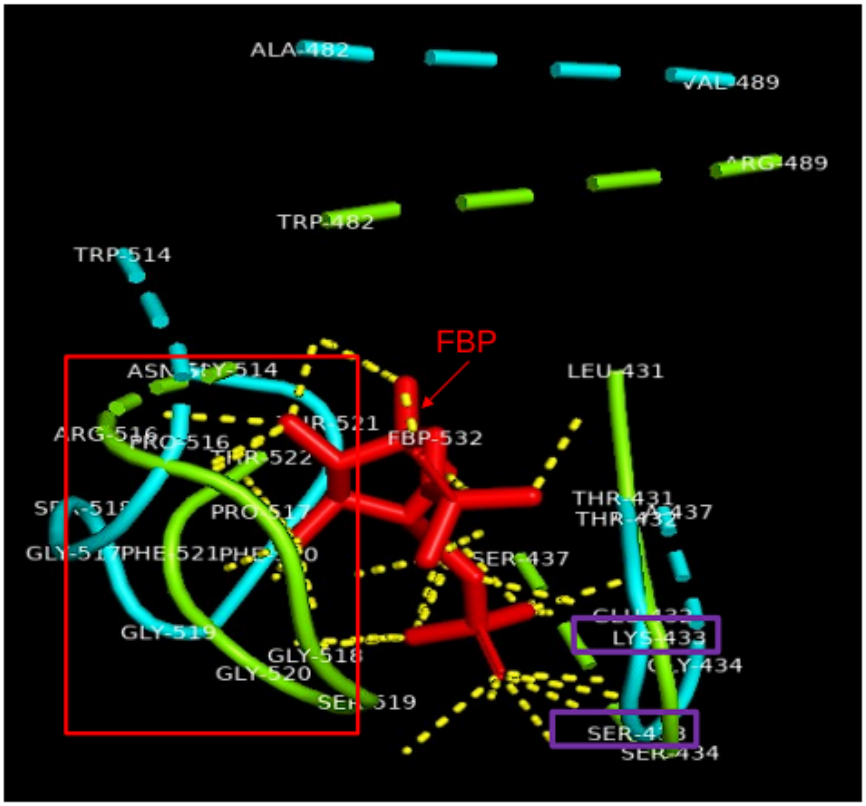

Figure 7: **Structural representation of the allosteric site of PKM isoforms.** Cartoon model of the amino acid composing the FBP allosteric site and comparison between PKM1 (in blue) and PKM2 (in green) in presence of FBP (in red). Important sites are colored to highlight their importance in the binding of FBP: the red square represents a regulatory loop and the violet square the residue 433 (Lys for PKM2 and Ser for PKM1).

List of Figures

1 **Global analysis of the RMSD vs RG shows structural changes and of the PKM2 volume during the oligomerization process. We also analyze PKM1/2 profile similarities. (A-D)** Graphical representation of the RMSD/RG analysis for each states of PKM2 molecular dynamics simulation : monomer **(A)**, dimer **(B)** and free-tetramer **(C)** or associated to FBP **(D)**, **(E)** Same representation for the tetrameric form of PKM1. 8

2 **The RMSF analysis shows PKM2's structuring during the oligomerization and FBP-fixation processes and confirms tetrameric PKM1/2 analogies on key domains. (A-D)** Graphical representation of the RMSF analysis for each state of PKM2 molecular dynamics: monomer **(A)**, dimer **(B)** and free-tetramer **(C)** or associated to FBP **(D)**, **(E)** Same representation for the tetrameric form of PKM1. Here the PKM2 domains contain the following residues : 44-115 for A1, **116-217 for B (red square)**, 218-388 for A2 and 389-531 for C-domain. Local differences between apo and holo PKM2 forms bound to FBP (green arrows), and between holo form of PKM2 bound to FBP and PKM1 respectively (red arrows) are indicated. 9

3 **The structuring of the active site is linked to the oligomeric conformation of PKM1/2. (A-E)** Graphical representation of the distance between residues 53 and 128 (in the active site) for each state of PKM2 within the simulations of the monomer **(A)**, dimer **(B)** and tetramer-apo **(C)** or holo PKM2 with FBP **(D)**, but also for the tetrameric state of PKM1 **(E)**, **(F-I)** Same representation for residues 178 and 296 with the monomer **(F)**, dimer **(G)** and apo **(H)** or holo-FBP **(I)** but also for the tetramer of PKM1 **(J)** 13

4 **Global structuring of the FBP-fixation pocket during PKM2 oligomerization and FBP-docking process and comparison with PKM1 possible fixation site.** **(A-D)** Graphical representation of the distance between residues 433 and 518 (localized at the FBP-allosteric pocket) for each oligomeric state or condition of PKM2 molecular dynamics with the monomer **(A)**, dimer **(B)** and tetramer-free **(C)** or associated with the allosteric molecule FBP **(D)**, **(E)** Same representation for the tetrameric form of PKM1. 16

5 **Structural data associated to the TEPP-46 fixation on a tetrameric PKM2.** **(A)** Graphical representation of the RMSF analysis, **(B)**, distance between residues 53 and 128 (in the active site) and **(C)** distance between residues 433 and 518 (localized at the FBP-allosteric pocket) for different tetrameric state of PKM2 with or without natural or pharmacological effectors. 19

6 **Structural representation of the active site of PKM2.** Cartoon model representing a single monomer of the PKM2 tetramer associated with FBP. Here, the two couple of residues **P53 to T129 (between regions A and B) and D178 to D296 (close to the A-B junction at the base of region B)) are highlighted respectively in blue and pink** to characterize their importance in the overall structural dynamics occurring at the active site of the protein, which is localized between the A1 (right side) and B-domains (left-side) 27

7 **Structural representation of the allosteric site of PKM isoforms.** Cartoon model of the amino acid composing the FBP allosteric site and comparison between PKM1 (in blue) and PKM2 (in green) in presence of FBP (in red). Important sites are colored to highlight their importance in the binding of FBP: the red square represents a regulatory loop and the violet square the residue 433 (Lys for PKM2 and Ser for PKM1). 28

References

(1) Morten, B.; al. Aerobic glycolysis in cancers: Implications for the usability of oxygen-responsive genes and fluorodeoxyglucose-PET as markers of tissue hypoxia. *International Journal of Cancer* **2008**, *122*, 2726–2734.

(2) Y, L. S.; G., V. H. M. Aerobic Glycolysis: Meeting the Metabolic Requirements of Cell Proliferation. *Annu. Rev. Cell Dev. Biol.* **2011**, *27*, 441–464.

(3) Emy, B.; Claudio, R. Signalling, Metabolic Pathways and Iron Homeostasis in Endothelial Cells in Health, Atherosclerosis and Alzheimer's Disease. *Cells* **2020**, *9*, 2073–4409.

(4) Kiichi, I.; Takehiko, T. Multimolecular Forms of Pyruvate Kinase from Rat and Other Mammalian Tissues*: I. Electrophoretic Studies. *The Journal of Biochemistry* **1972**, *6*, 1043–51.

(5) T, N.; al. The M1- and M2-type isozymes of rat pyruvate kinase are produced from the same gene by alternative RNA splicing. *Journal of Biological Chemistry* **1986**, *261*, 13807–13812.

(6) Israelsen, W. J.; Heiden, M. G. V. Pyruvate kinase: function, regulation and role in cancer. *Seminars in cell & developmental biology 43* **2015**, 43–51.

(7) Barbara, C.; al. Pyruvate kinase expression (PKM1 and PKM2) in cancer-associated fibroblasts drives stromal nutrient production and tumor growth. *Cancer biology therapy* **2011**, *12*, 1101–1113.

(8) Clover, C. V.; al. The alternative splicing repressors hnRNP A1/A2 and PTB influence pyruvate kinase isoform expression and cell metabolism. *Proceedings of the National Academy of Sciences of the United States of America* **2010**, *5*, 1894–99.

(9) Takenaka, M.; al. Isolation and Characterization of the Human Pyruvate Kinase M Gene. *European Journal of Biochemistry* **1991**, *1*, 101–6.

(10) Morgan, H. P.; al. M2 pyruvate kinase provides a mechanism for nutrient sensing and regulation of cell proliferation. *Proceedings of the National Academy of Sciences 110* **2013**, *15*, 5881–86.

(11) Weiwei, Y.; Lu., Z. Nuclear PKM2 regulates the Warburg effect. *Cell cycle* **2013**, *12,19*, 3154–8.

(12) Yoshitaka Ikeda, T. T.; Noguchi, T. Conversion of Non-Allosteric Pyruvate Kinase Isozyme into an Allosteric Enzyme by a Single Amino Acid Substitution. *Journal of Biological Chemistry 272* **1997**, *33*, 20495–501.

(13) Yuan, M.; al. « An allostatic mechanism for M2 pyruvate kinase as an amino-acid sensor. *Biochemical Journal 475* **2018**, *10*, 1821–37.

(14) Kirstie E. Keller, I. S. T.; Lee, Y.-S. « SAICAR Stimulates Pyruvate Kinase Isoform M2 and Promotes Cancer Cell Survival in Glucose -Limited Conditions. *Science (New York, N.Y.) 338* **2012**, *6110*, 1069–72.

(15) Jurica, M. S.; al. The Allosteric Regulation of Pyruvate Kinase by Fructose-1,6-Bisphosphate. *Structure 6* **1998**, *2*, 195–210.

(16) Kato, H.; al. « Cytosolic Thyroid Hormone-Binding Protein is a Monomer of Pyruvate Kinase. *Proceedings of the National Academy of Sciences of the United States of America 86* **1989**, *20*, 7861–65.

(17) Jill D. Dombrauckas, B. D. S.; Mesecar, A. D. Structural Basis for Tumor Pyruvate Kinase M2 Allosteric Regulation and Catalysis. *Biochemistry 44* **2005**, *27*, 9417–29.

(18) Anastasiou, D.; al. « Pyruvate kinase M2 activators promote tetramer formation and suppress tumorigenesis. *Nature chemical biology 8* **2012**, *10*, 839–47.

(19) Thonsri, U.; al. Antitumor Effect of Shikonin, a PKM2 Inhibitor, in Cholangiocarcinoma Cell Lines. *Anticancer Research 40* **2020**, *9*, 5115–24.

(20) Gresh, N.; Cisneros, G. A.; Darden, T. A.; Piquemal, J.-P. Anisotropic, Polarizable Molecular Mechanics Studies of Inter- and Intramolecular Interactions and Ligand-Macromolecule Complexes. A Bottom-up Strategy. *Journal of Chemical Theory and Computation* **2007**, *3*, 1960–1986, PMID: 18978934.

(21) Shi, Y.; Ren, P.; Schnieders, M.; Piquemal, J.-P. *Reviews in Computational Chemistry Volume 28*; John Wiley & Sons, Ltd, 2015; Chapter 2, pp 51–86.

(22) Melcr, J.; Piquemal, J.-P. Accurate Biomolecular Simulations Account for Electronic Polarization. *Frontiers in Molecular Biosciences* **2019**, *6*, 143.

(23) Jing, Z.; Liu, C.; Cheng, S. Y.; Qi, R.; Walker, B. D.; Piquemal, J.-P.; Ren, P. Polarizable Force Fields for Biomolecular Simulations: Recent Advances and Applications. *Annual Review of Biophysics* **2019**, *48*, 371–394, PMID: 30916997.

(24) Adjoua, O.; al. Tinker-HP: Accelerating Molecular Dynamics Simulations of Large Complex Systems with Advanced Point Dipole Polarizable Force Fields Using GPUs and MultiGPU Systems. *Journal of Chemical Theory and Computation 17* **2021**, *4*, 2034–53.

(25) Lagardère, L.; al. Tinker-HP: A Massively Parallel Molecular Dynamics Package for Multiscale Simulations of Large Complex Systems with Advanced Point Dipole Polarizable Force Fields. *Chemical Science 9* **2018**, *4*, 956–72.

(26) Inizan, T. J.; al. High-Resolution Mining of the SARS-CoV-2 Main Protease Conformational Space: Supercomputer-Driven Unsupervised Adaptive Sampling. *Chemical Science 12* **2021**, *13*, 4889–4907.

(27) Dina, E. A.; al. Interfacial Water Many-Body Effects Drive Structural Dynamics and Allosteric Interactions in SARS-CoV-2 Main Protease Dimerization Interface. *J. Phys. Chem. Lett.* **2021**, *12*, 6218–6226.

(28) El Khoury, L. et al. Computationally driven discovery of SARS-CoV-2 Mpro inhibitors: from design to experimental validation. *Chem. Sci.* **2022**, *13*, 3674–3687.

(29) Srivastava, D.; al. Structural Investigation of a Dimeric Variant of Pyruvate Kinase Muscle Isoform 2. *Biochemistry* **2017**, *2017*, 6517–20.

(30) Dimitrios, A.; al. Pyruvate kinase M2 activators promote tetramer formation and suppress tumorigenesis. *Nature chemical biology 8* **2012**, *10*, 839–47.

(31) Ren, P.; Ponder, J. W. Polarizable Atomic Multipole Water Model for Molecular Mechanics Simulation. *The Journal of Physical Chemistry B 107* **2003**, *24*, 5933–47.

(32) Shi, Y.; al. « The Polarizable Atomic Multipole-based AMOEBA Force Field for Proteins. *Journal of chemical theory and computation 9,* **2013**, *9*, 4046–63.

(33) Wu, J. C.; al. Automation of AMOEBA polarizable force field parameterization for small molecules. *Theor Chem Acc* **2012**, *131*, 1138.

(34) Walker, B.; al. Automation of AMOEBA Polarizable Force Field for Small Molecules: Poltype 2. *Journal of Computational Chemistry* **2022**, *43*, 1530–1542.

(35) Nandi, S.; al. Structural Basis for Allosteric Regulation of Pyruvate Kinase M2 by Phosphorylation and Acetylation. *Journal of Biological Chemistry 295* **2020**, *51*, 17425–40.

(36) Joshua, R.; al. Tinker 8: Software Tools for Molecular Design. *J. Chem. Theory Comput.* **2018**, *14*, 5273–5289.

(37) Louis Lagardère, A. F.; Jean-Philip, P. Pushing the Limits of Multiple-Time-Step Strategies for Polarizable Point Dipole Molecular Dynamics. *J. Phys. Chem. Lett.* **2019**, *10*, 2593–99.

(38) W, H. C.; al. Long-Time-Step Molecular Dynamics through Hydrogen Mass Repartitioning. *J. Chem. Theory Comput.* **2015**, *11*, 1864–74.

(39) Lagardère, L.; Lipparini, F.; Polack, ; Stamm, B.; Cancès, ; Schnieders, M.; Ren, P.; Maday, Y.; Piquemal, J.-P. Scalable Evaluation of Polarization Energy and Associated Forces in Polarizable Molecular Dynamics: II. Toward Massively Parallel Computations Using Smooth Particle Mesh Ewald. *Journal of Chemical Theory and Computation* **2015**, *11*, 2589–2599, PMID: 26575557.

(40) Åqvist, J.; al. Molecular dynamics simulations of water and biomolecules with a Monte Carlo constant pressure algorithm. *Chemical Physics Letters* **2004**, *384*, 288–294.

(41) Bowman, G. R.; al. Enhanced Modeling via Network Theory: Adaptive Sampling of Markov State Models. *J. Chem. Theory Comput.* **2010**, *6*, 787–94.

(42) Pedregosa, F.; al. Scikit-Learn: Machine Learning in Python. *arXiv* **2018**,

(43) McGibbon, R. T.; al. MDTraj: A Modern Open Library for the Analysis of Molecular Dynamics Trajectories. *Biophysical Journal* **2015**, *8*, 1528–32.

(44) Harris, C. R.; al. Array programming with NumPy. *Nature* **2020**, *7825*, 357–62.

(45) Virtanen, P.; al. SciPy 1.0: Fundamental Algorithms for Scientific Computing in Python. *Nature Methods* **2020**, *3*, 261–72.

(46) Hunter, J. D. Matplotlib: A 2D Graphics Environment. *Computing in Science Engineering* **2007**, *3*, 90–95.

(47) Ponnusamy, N. S., Kalaiarasan; Bamezai., R. Molecular simulation of Tyr105 phosphorylated pyruvate kinase M2 to understand its structure and dynamics. *Journal of molecular modeling 20* **2014**, 2447.

(48) Zhang, Z.; al. PKM2, function and expression and regulation. *Cell & Bioscience 9* **2019**, *1*, 52.

(49) Xie, C. D., Jiansheng; Hu., X. Evidence That Does Not Support Pyruvate Kinase M2 (PKM2)-catalyzed Reaction as a Rate-limiting Step in Cancer Cell Glycolysis. *The Journal of Biological Chemistry 291* **2016**, *17*, 8987–99.

(50) Jianshuand, G.; al. Dimethylaminomicheliolide (DMAMCL) Suppresses the Proliferation of Glioblastoma Cells via Targeting Pyruvate Kinase 2 (PKM2) and Rewiring Aerobic Glycolysis. *Frontiers in Oncology* **2019**, *9*, 993.

(51) Wang Ping, T. Z., Chang Sun; Xu., Y. Structural insight into mechanisms for dynamic regulation of PKM2. *Protein & cell 6* **2015**,

(52) Xueliang, G.; al. Pyruvate Kinase M2 Regulates Gene Transcription by Acting as A Protein Kinase. *Molecular Cell 45* **2012**, *5*, 598–609.

(53) Zahra, K.; al. Pyruvate Kinase M2 and Cancer: The Role of PKM2 in Promoting Tumorigenesis. *Frontiers in Oncology* **2020**, *10*, 2234–943X.

(54) Jingxu, Y.; al. Synergistic Allosteric Mechanism of FBP and Serine for Pyruvate Kinase M2 via Dynamics Fluctuation Network Analysis. *Journal of chemical information and modeling 56* **2016**, *6*, 1184–92.

(55) P., M. H.; al. Allosteric Mechanism of Pyruvate Kinase from Leishmania Mexicana Uses a Rock and Lock Model. *Journal of Biological Chemistry 285* **2010**, *17*, 12892–98.

(56) Heather, C.; al. Pyruvate kinase M2 is a phosphotyrosine-binding protein. *Nature 452* **2008**, 181–86.

(57) Hong-Sheng, Z.; al. PKM2-mediated inhibition of autophagy facilitates Tat's inducing HIV-1 transactivation. *Biochemistry and Biophysics* **2017**, *625-626*, 17-23.

(58) Kwok-Fung, L. A.; al. Activation of the FGFR1 signalling pathway by the Epstein–Barr virus-encoded LMP1 promotes aerobic glycolysis and transformation of human nasopharyngeal epithelial cells. *The Journal of Pathology* **2015**, *237*, 238–248.